KOSZALIN UNIVERSITY OF TECHNOLOGY
POLITECHNIKA KOSZALIŃSKA

Monograph

RESEARCH AND MODELLING IN CIVIL ENGINEERING 2017

Edited by
Jacek Katzer and Krzysztof Cichocki

KOSZALIN 2017

MONOGRAPH NO 338
FACULTY OF CIVIL ENGINEERING,
ENVIRONMENTAL AND GEODETIC SCIENCES

ISSN 0239-7129
ISBN 978-83-7365-474-7

Chairman of the University Editorial Board
Zbigniew Danielewicz

Editors
Jacek Katzer, Krzysztof Cichocki
Koszalin University of Technology, Poland

Reviewers
Jacek Gołaszewski – Silesian University of Technology, Poland
Izabela Major – Częstochowa University of Technology, Poland

Technical editor
Czesław Suchocki

Website editor
Mariusz Ruchwa

Linguistic consultations
Ewa Sokołowska-Katzer

Typesetting
Czesław Suchocki

Cover design
Tadeusz Walczak
(Photo by *Jacek Katzer*)

KOSZALIN UNIVERSITY OF TECHNOLOGY PUBLISHING HOUSE
75-620 Koszalin, Racławicka 15-17, Poland

Koszalin 2017, 1st edition, publisher's sheet 7,8, circulation 100 copies
Printing: INTRO-DRUK, Koszalin, Poland

Table of contents

1. Energy transfer improvement in a water pumping installation 7

2. Dynamic numerical analysis of the integrated shear connection..... 23

3. Effect of carbon nanotubes on the mechanical fracture properties of alkali-activated materials 37

4. A correction of fatigue characteristics of concrete with respect to age of specimens..... 51

5. Selected applications of acoustic methods in building materials monitoring 63

6. Comprehensive Monitoring of the Shrinkage and Structural Changes of Cement Composites during Setting and Hardening..... 81

7. Impedance spectroscopy, a method to determine physical and chemical properties of construction materials..... 99

8. Simulation quality of the probability of the reinforced concrete corrosion initiation evaluation 115

9. Multi-parameter fracture mechanics: Practical use 133

10. Selected problems of the foundation slab under the residential building.. 145

5. Selected applications of acoustic methods in building materials monitoring

Libor Topolář[1], Luboš Pazdera[2], Michaela Hoduláková[3], Karel Mikulášek[4]
[1,2,3,4] Brno University of Technology, Faculty of Civil Engineering, Brno, Czech Republic,

5.1. Introduction

Non-destructive testing (NDT) is a process of inspecting, testing, and evaluating materials, components or assemblies for discontinuities, or differences in characteristics without destroying the serviceability of a system or its part. In other words, after an inspection or test is completed the part inspected can still be used.

The acoustic NDT methods are concerned with the state-of-the-art situation in the field of experimental studies of the physical properties of engineering materials. The evaluation of these properties has been a longstanding urgent problem in civil engineering and its importance is constantly increasing with the advent of novel types of engineering materials.

NDT methods are advantageous with its capacity to detect cracks and pores in building materials. In addition, they produce good results in the testing of such materials as metals and composites. The following are their major advantages: acceptable accuracy, safety in experiments, low cost, and the easy transportability of equipment to the place where the actual measurements are performed.

However, applying acoustic NDT to building composites poses certain difficulties due to their complex internal structure. An engineering material can be regarded as a composite of composites, it is inhomogeneous at the micro and macro levels, and can be characterized by such opposite properties as brittleness and softness, elasticity and inelasticity, properties that are characteristic of a liquid (fluidity) and a solid (shear strength), the presence of cracks, cavities, and pores that are filled with air or liquid (or with both air and liquid) (Brigante 2013).

Non-destructive acoustic analysis methods, the Impact Echo (IE) method as a traditional and the Acoustic Emission (AE) method as the non-traditional method for civil engineering, were used in several experiments.

5.2. Acoustic Emission Method

The AE method has been regarded as the prime candidate for structural health and damage monitoring in loaded structures for many years. It offers the user a number of inherent advantages; mainly, it is able to continuously monitor in situ and to examine the whole volume of a structure simultaneously with a limited number of sensors (Iturrioz 2014). Acoustic emission refers to the noise emitted by material and structures when subjected to stress. The stress types can be mechanical, thermal, or chemical. The emission is caused by rapid release of energy within a material due to events such as crack formation, and the subsequent extension occurring under an applied stress, generating transient elastic waves, which can be detected by piezoelectric sensors (Grosse 2008, Ohtsu 1996).

The main AE parameters (Surgeon 1999):

- Count - the number of times an AE signal crosses the threshold
- Duration - difference between the first and the last time an AE signal crosses the threshold
- Amplitude - maximum/minimum voltage excursion of an AE signal within duration

AE activity is attributed to the rapid release of energy in a material with the energy content of the AE signal being related to this energy release. The true energy is directly proportional to the area under the AE waveform (Sagar 2009):

$$AE\ energy_i = \int_{t_0}^{t_1} V_i(t)^2 dt \tag{5.1}$$

where:

i – the recorded voltage transient $V(t)$ of a channel
t_0 – the starting time of the voltage transient record
t_1 – the ending time of the voltage transient record

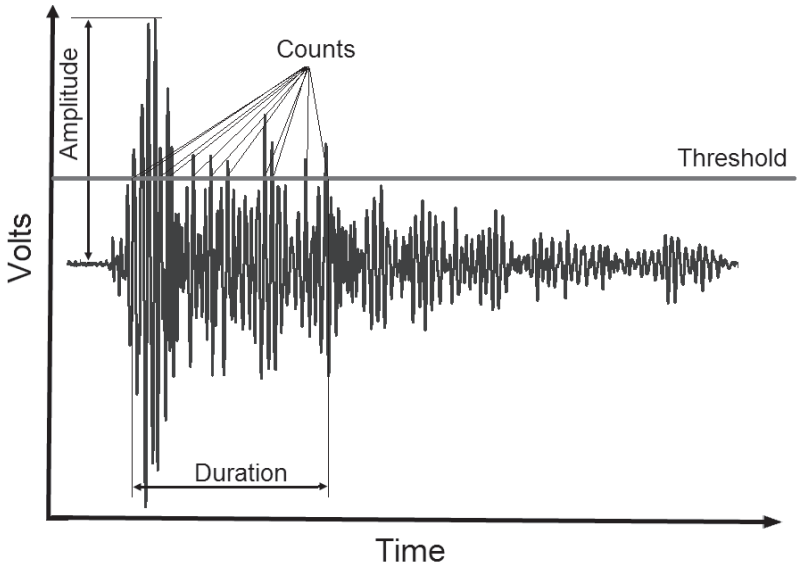

Fig. 5.1. Typical AE event

Various types of cracks generate different types of AE signals with varying parameters, such as frequencies and amplitudes. These differences can be related to the degree of damage to the structure or material composition. The smaller microcracks generate many small amplitude events while the bigger ones generate fewer events but with higher amplitudes. When the cracks are opening, as most of the energy has already been released, many events with small amplitudes are created. Furthermore, tensile cracks spawn large amplitude events while shear cracks create smaller amplitude signals (Iwanami 1997, Li 1995).

Acoustic emission equipment

To detect AE signals in experiments, a DAKEL XEDO measurement system was used consisting of AE sensors (MDK13 with inbuilt magnetic holder, IDK 09 and MTPA-15 with inbuilt preamplifier approx. 35 dB), amplifier (AS3K with 35 dB gain), and filter (100-800 kHz). The total amplification of the preamplifier and the main amplifier was set at 55 to 75 dB. The measurement system records such parameters as count, hit, event, maximum amplitude, rise time, duration, root mean square (RMS), and voltage and arrival-time difference. The waveform parameters are illustrated in Figure 5.1. Elimination of the noise is ensured by setting the threshold level at 200 - 400 mV according to the configuration of a particular experiment, or by filtering in a post-analysis of the data.

5.3. Impact-echo Method

As a non-destructive acoustic technique based on the idea that the mechanical characteristics of a specimen affect its spectral properties, the IE method analyzes

the elastic impulse-induced mechanical wave (Liang 2001). A short-time mechanical impulse induced by a steel spherical body gives rise to a low-frequency pressure wave (Fig. 5.2). Thus, the generated wave propagates through the specimen's structure being rebounded by defects located in the specimen's bulk or on its surface. The time difference between the emitted and the rebounded waves is recorded by a sensor, which shows the signal waveform. In theory, the impact resembles a delta-function containing all possible frequencies. During wave propagation, each frequency component is affected by the geometry of the specimen, the material properties, defects, non-homogeneities, cracks or any other structural characteristics (Birgham 1988). The frequency spectrum of the gathered signal is calculated using Fast Fourier Transform (especially its dominant frequencies) giving an account of the condition of the specimen.

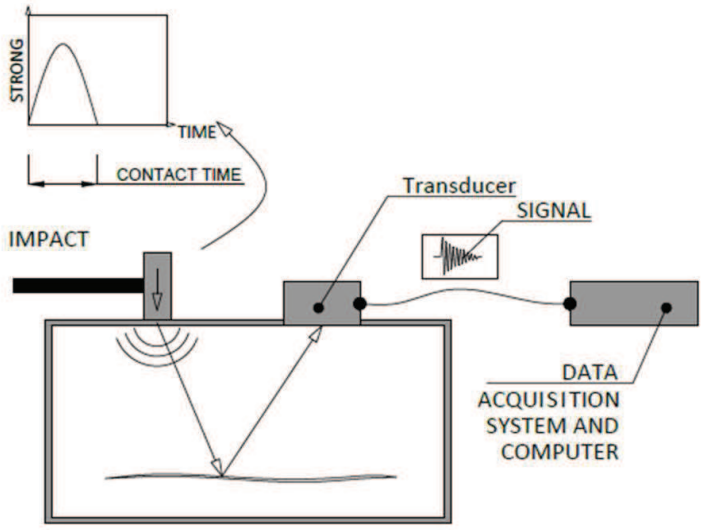

Fig. 5.2. Principle of the Impact Echo method

Impact-echo measurement

In order to generate the signal, a hammer of 12 g mass, originally suspended from a hanger, was released to fall down on the specimen from a height of 4 cm. The impulse was reflected by the surface but also by microcracks and defects of the specimen under investigation. The response was picked up by a MIDI type piezoelectric sensor. Its output voltage was fed into a TiePie engineering Handyscope HS3, which is a two-channel, digital, 16 bits oscilloscope. The piezoelectric sensor was placed at the end of the beam at the centre of the transverse side and the hammer hit was carried out on the opposite side in the direction of the longitudinal axis. The sensor was attached to the surface of the specimen by beeswax. Subsequently, a special smoothing algorithm was used to determine the dominant frequencies for each of the output signals.

5.4. Achieved results and discussion

5.4.1. Measurement during setting and hardening using waveguides

We studied a cement-based beam sized 360 mm x 50 mm x 50 mm. For the beam, fine-grained concrete mixture was used composed of 400 kg cement CEM II/B – S 32.5 and 1400 kg sand Želešice with the fraction of aggregate being 0 mm – 4 mm and 225 l water. The fine-grained concrete was modified on a vibration table. After casting, the fine-grained concrete was kept in the forms at room temperature for 24 hours before demoulding. Two specimens were measured simultaneously for each method. One specimen was sealed by PE foil to avoiding water exchange with the environment and the specimen was cured without any water exchange prevention. The second specimen was left free in the air without treatment. Four AE sensors were placed on the surface of both specimens (see Fig. 5.5. - left). Two sensors were placed on the first specimen and another two on the second one. For the IE method, the piezoelectric sensor was placed at one beam end in the longitudinal centre line of the beam and the hammer hit the opposite end of the beam in the direction of the centre line of the beam (see Fig. 5.3 - right).

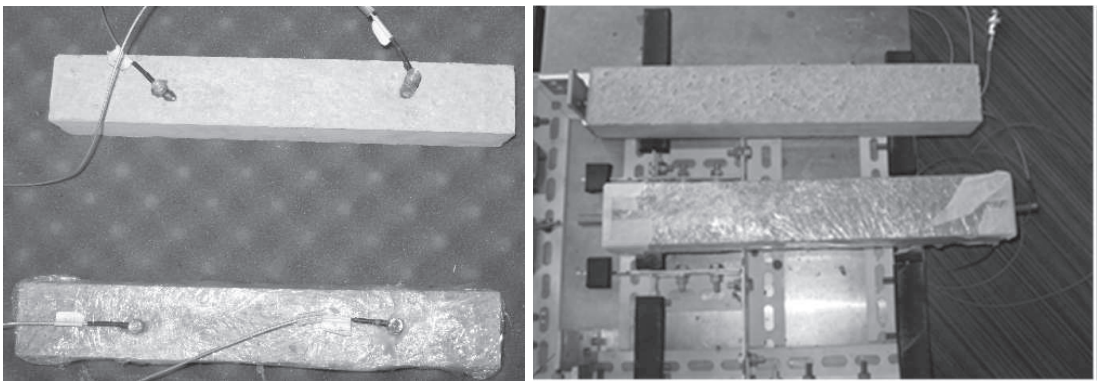

Fig. 5.3. Photography of Acoustic Emission (left) and Impact-echo (right) measurement

The measurement began after demoulding, that is, 24 hours later by preparing the fine-grained concrete mixture. The diagram in Fig. 5.4 shows how the cumulative count N_C depends on time t. The foil-covered specimen (solid line) had a significantly lower AE count than the specimen without cover (dashed line) during the measurement period (10 days). The higher AE activity is likely to be caused by a higher number of microcracks in the specimen (Pazdera 2010).

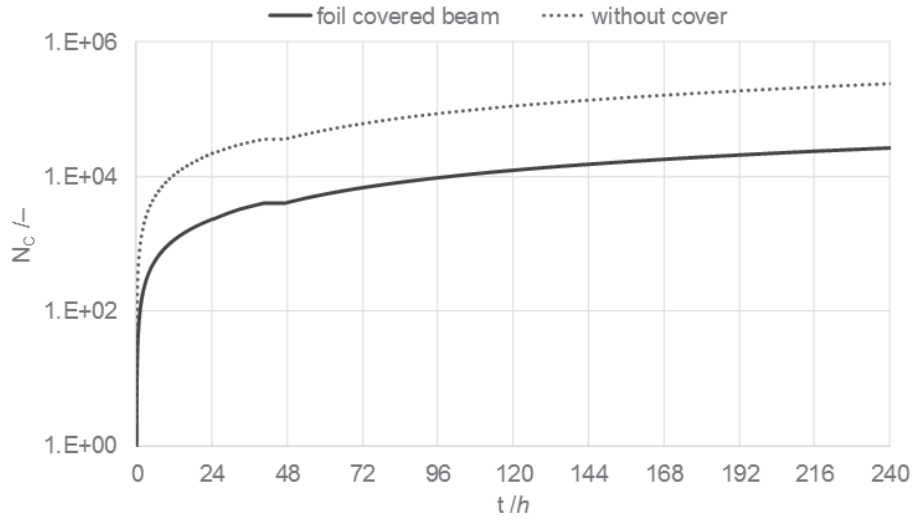

Fig. 5.4. Time-dependent cumulative counts of acoustic emission (N_C)

The graphs (Fig. 5.5 and Fig. 5.6) show the frequency spectrum. For two specimens (foil covered beam and beam without cover), each graph is shown at a different time from the moment of mixing.

Fig. 5.5 shows the frequency spectrum for specimens at the beginning the fine-grained concrete (that is, 24 hours after mixing). In the frequency spectrum, the foil covered specimen (solid line) has the frequency (marked A) at position 990 Hz. This frequency A is not visible in the specimen without cover (dashed line). During the hardening, the frequency A moved to the value of 1430 Hz (after 240 hours of mixing) as shown in Fig. 5.6. Another significant frequency (labelled B) only occurs during the monitoring of the foil cover specimen again. 24 hours after mixing (Fig. 5.5) it had a value of 2870 Hz and, after 240 hours of mixing (Fig. 5.6), this increased to 3230 Hz.

The frequency (marked C - foil cover specimen; C' - without cover specimen) is present in both specimens. The foil-cover specimen's frequency C within 24 hours after mixing was 3630 Hz and, at the end of monitoring, 5160 Hz. The corresponding frequency C' of the specimen without cover after 24 hours from mixing was 3390 Hz while, at the end of monitoring, its value was 4510 Hz. From this frequency, we can find the frequencies of higher orders which might indicate that it is a self-resonant frequency of the specimen.

At the end of the monitoring (that is, after 240 hours from mixing) 3 significant frequencies (marked X ', Y', Z ') were found in the specimen without cover, see Fig. 5.6. These frequencies were probably formed due to the non-linearities in the structure of the element. These non-linearities are due to the lack of water during the hydration of cement and, probably, cause damage to the structure of the specimen.

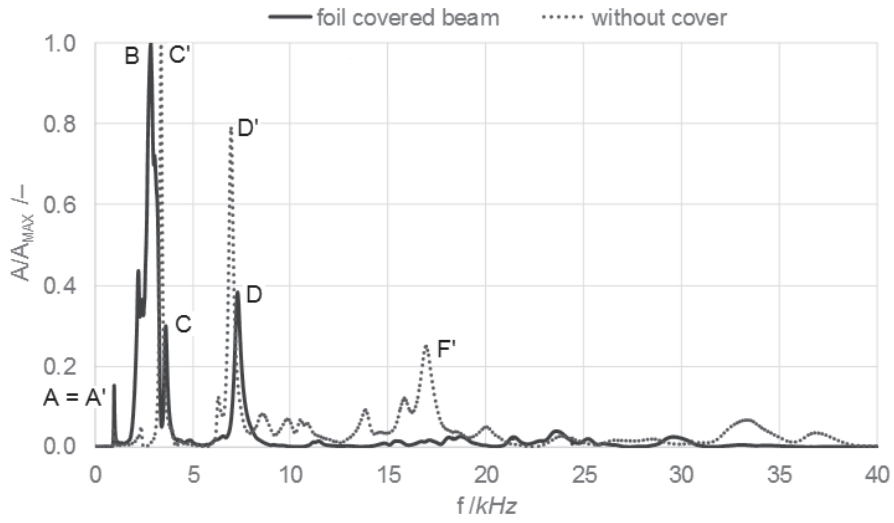

Fig. 5.5. Impact Echo – frequency spectrum 24 hours after the mixing

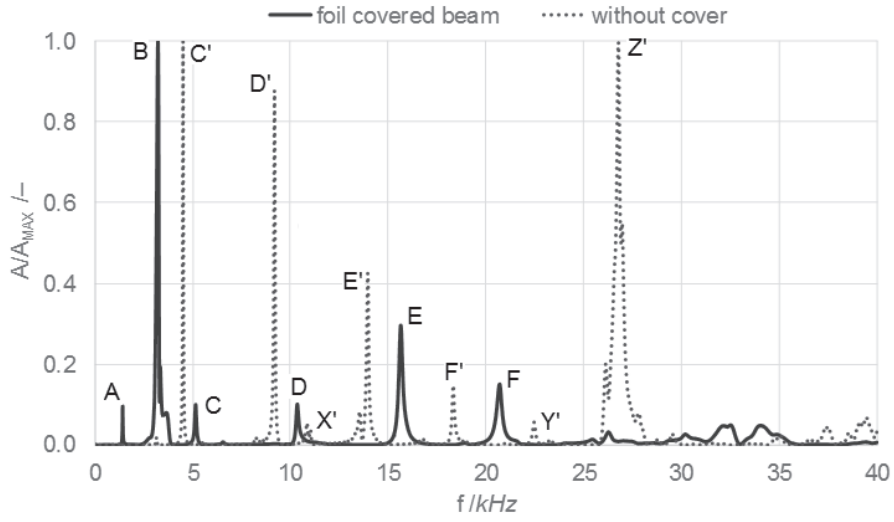

Fig. 5.6. Impact Echo – frequency spectrum 240 hours after the mixing

The diagram in Fig. 5.7 shows the dependence of weight loss m on time t. The foil-covered specimen (solid line) has a significantly lower weight loss than the one without cover (dashed line) during the measurement period (10 days). The foil-covered specimen used all the water added to the batch during mixing. The weight loss of the specimen without cover is caused by both the hydration and water evaporation.

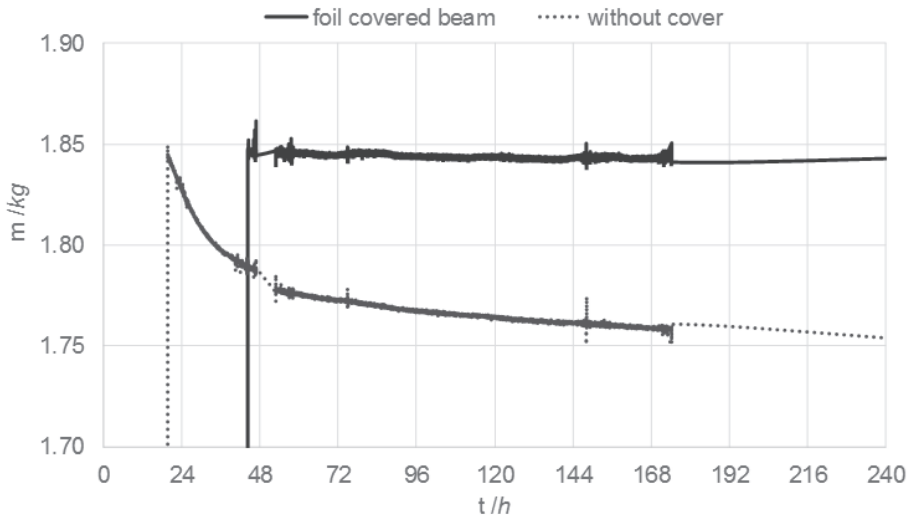

Fig. 5.7. The time (t)-dependent weight loss of the specimen (m).

5.4.2. The pilot measurement during the six freeze-thawing cycles

Two specimens sized 100 x 100 x 400 mm were measured simultaneously. Four AE sensors were placed on the surface of both specimens (see Fig. 5.8). Two sensors were placed on the first specimen and another two on the second one. Each sensor was kept in place by a specifically made holder for the contact between the sensor and the specimen surface to be as good as possible.

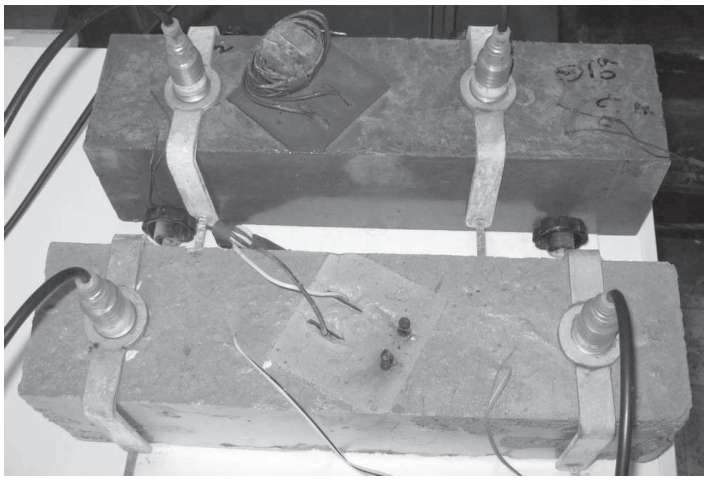

Fig. 5.8. Location of acoustic emission and temperature sensors and electrodes for monitoring electrical properties

The sensors are designed to be resistant to an aggressive salt solution and can be applied in temperatures from -30 to +30 °C without any problems (Zhang 2006). Both specimens were put into a freezer until the temperature fell down to -25 °C. Then, they were put into water with a temperature of 15 ~ 20 °C. As this was a

pilot measurement, everything was done manually. For this reason, some of the longer cycles are shorter. To compare both specimens and test methods for this type of building material failure, the experiment was sufficient.

Temperatures T (°C) inside the specimens were measured by negative thermal resistors during the whole experiment being computed using the equation:

$$T = 0.03 \cdot \left(\frac{R_x}{R_{25}}\right)^4 - 0.83 \cdot \left(\frac{R_x}{R_{25}}\right)^3 + 7.49 \cdot \left(\frac{R_x}{R_{25}}\right)^2 - 33.92 \cdot \left(\frac{R_x}{R_{25}}\right) + 51.69, \quad (5.2)$$

where R_x is the measured resistance (Ω), R_{25} is a reference resistance at 25 °C (Ω). These sensors were embedded in concrete specimens.

The graphs in Fig. 5.9 and Fig. 5.10 show cumulative counts (N_C) and temperatures (T) over time (t). For the specimen with worse frost resistance, a significantly higher AE count was observed than for the one with better frost resistance during the measurement period (6 freeze-thaw cycles). It can be assumed that the greater numbers of counts are caused by higher numbers of microcracks in the specimen. Higher AE activity is observed as he temperature increases. As the temperature decreases the AE, the activity does not usually change very much. AE activities, i.e., micro-changes in the structure, are indicated within one and a half day from the start of temperature increase (Pazdera 2014). Thus, when specimens were pulled out from the freezer, micro-changes had been in progress for two days. When specimens were put back in the freezer for another two days, the AE activities continued (see Figs. 5.9 and 5.10).

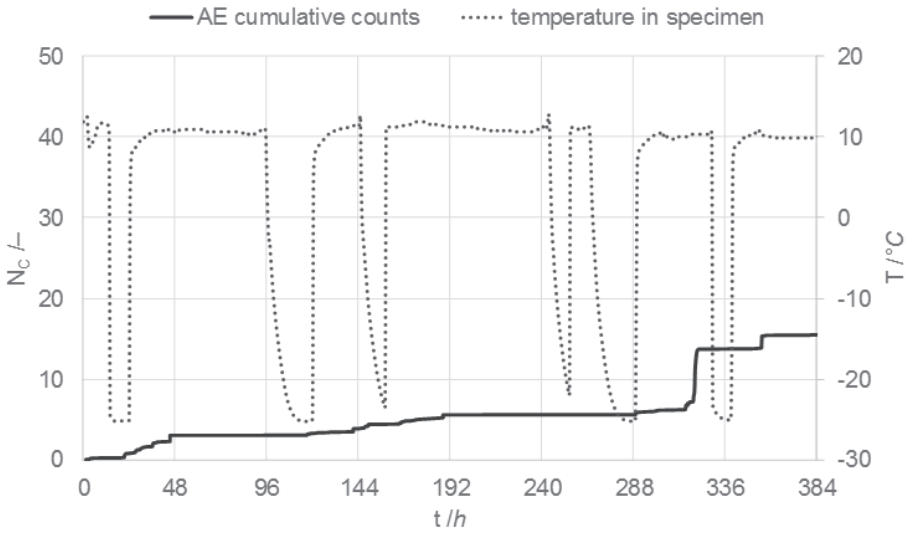

Fig. 5.9. The acoustic emission activity (N_C – left axis) and temperature (T - right axis) over time (t) - (specimen with better frost resistance)

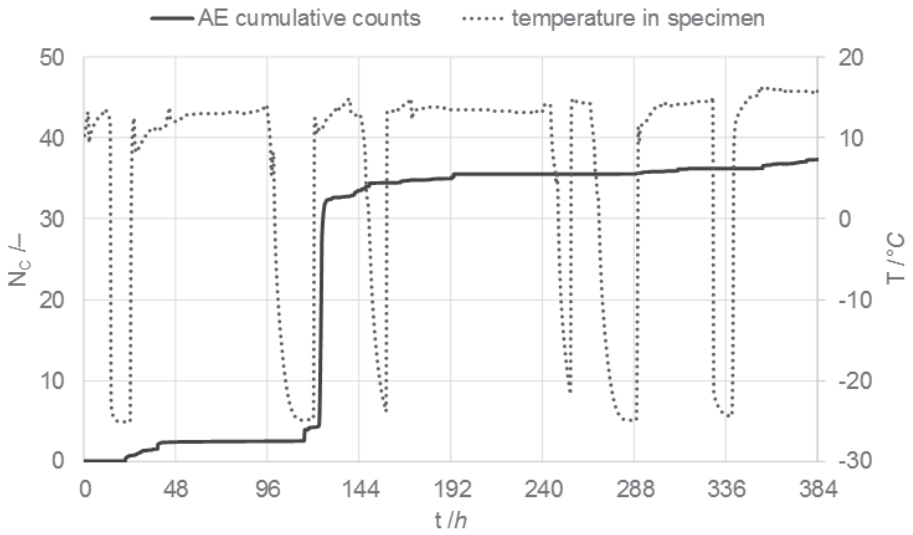

Fig. 5.10. Acoustic emission activity (N_C – left axis) and temperature (T - right axis) over time (t) - (specimen with worse frost resistance)

Both mixtures were monitored by the IE method, too. The specimen with better frost resistance (Fig. 5.11) shows two natural frequencies, f_1 = 2200 Hz and f_2 = 5500 Hz. Their positions after the application of six freezing cycles were similar. However, the frequency spectra of the specimen with worse frost resistance (Fig. 5.12) are different after six freezing cycles, which indicates a worse frost resistance of this specimen. The spectrum contained two frequencies, f_1 = 850 Hz and f_2 = 1990 Hz. After the degradation, these two frequencies were spread into seven frequency components. This is due to many small defects in the monitored structure.

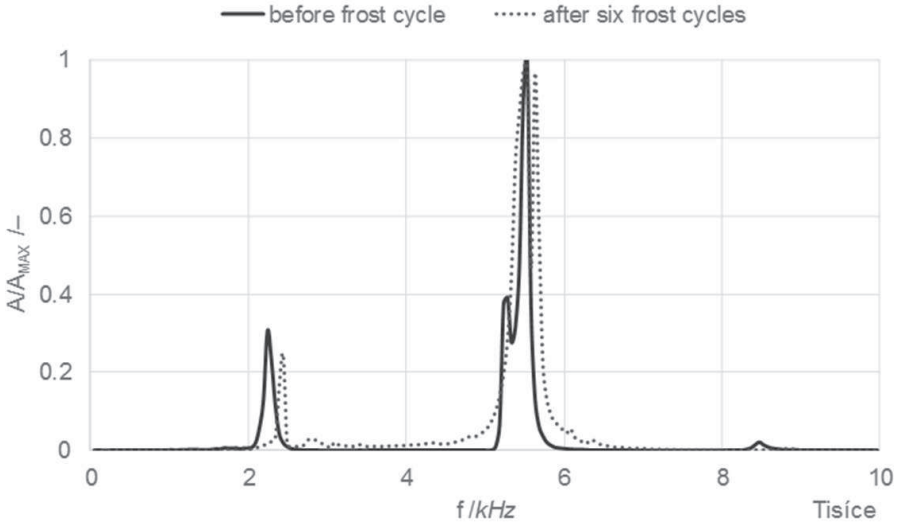

Fig. 5.11. Relative frequency spectrum of the concrete specimen with better frost resistance

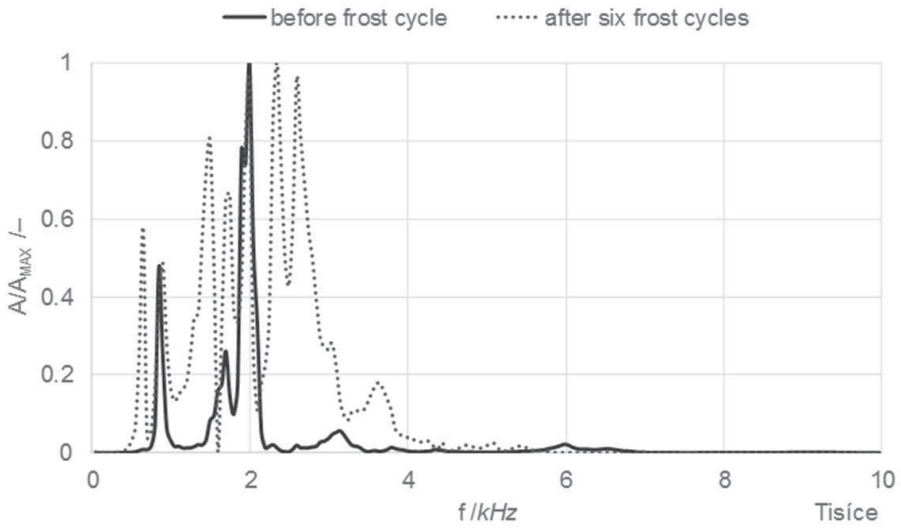

Fig. 5.12. Relative frequency spectrum of concrete specimen with worse frost resistance

5.4.5. Measurement of heat degradation specimens

For the experimental part, concrete specimens with dimensions of 100 x 100 x 400 mm were prepared. Seven sets of test specimens were manufactured. Each set was labelled with an ID number which corresponds to the temperature conditions maintained in the laboratory furnace during its heating. Specimens labelled 20 represent concrete specimens which dried freely in laboratory conditions with a temperature of (21±1) °C and were not further heated. The specimens (except for specimens labelled 20) were immersed in a water bath for 28 days. Then, they were dried first in the laboratory conditions and then in a ceramic furnace at temperature 110 °C for another 48 hours. The concrete specimens were heated in a programmable laboratory furnace Rhode KE 130B at the heating rate of 5 °C/min. Selected temperatures T= 200 °C, 400 °C, 600 °C, 800 °C, 1000 °C and 1200 °C were maintained for 60 minutes. Three-point bending (3PB) tests were performed after the specimens were exposed to prescribed thermal stress levels. Ten specimens from each set were tested. Four AE sensors were attached to the surface by beeswax – see in Fig. 5.15. The loading tests were carried out using a Heckert FPZ 100/1 testing machine at a laboratory in the Institute of Building Testing, Faculty of Civil Engineering, Brno University of Technology. Beam specimens with initial central edge notches were loaded under a 3PB test using the displacement-controlled method which is more suitable for monitoring the behaviour of specimens after crack initiation and during its propagation. The initial notch was made by a diamond blade sawed before testing. The depth of the notches was about 33 mm for all specimens (Topolář 2015).

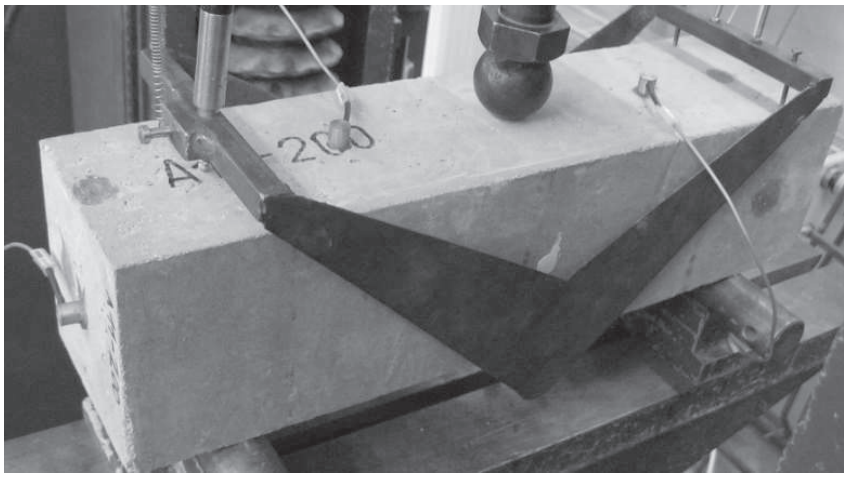

Fig. 5.15. The location of acoustic emission sensors on specimen during the three-point bending test

To describe AE signals which are formed during the three-point bending test in the specimens, the focus was on the number of events and AE energy. Fig. 5.14 and Fig. 5.15 present the dependence of the number of AE events on the thermal stress level. The waves which emerge and propagate within the specimen during the three-point bending test can affect the material element oscillations. The exposure to elevated temperatures causes a change of structure, leading to the change in the number of AE events. These changes can be accounted for by the process of concrete decomposition during the thermal stress application. Heating the concrete up to 100 °C results in the dehydration (loss of the chemically bound water) with the formation of Calcium-Silicate-Hydrate (C-S-H) and calcium hydroxide $Ca(OH)_2$ – Portlandite. As the temperature is further raised up to 200 °C, a dehydration of cementing compound begins resulting in the release of physically bound water along with the concurrent decomposition of hydrate. The first stage of decomposition of C-S-H and decomposition of gypsum $CaSO_4.2H_2O$ culminates between 150 °C and 170 °C. However, the number of AE events is lower than in the case of specimen labelled 20 (unheated), which indicates a lower quantity of new formed microcracks. At a temperature above 200 °C, physically bound water is released. Between 250 - 300 °C, the hydrated cement phases are decomposed. Further increase of temperature above 300 °C results in the decomposition of Portlandite [$Ca(OH)_2 \rightarrow CaO + H_2O$] and significant formation of microcracks. The formation of microcracks and Portlandite decomposition results in a significant increase in the amount of microcracks which arises before the ultimate tensile capacity of the test specimens during three-point bending test is reached. The decrease of the number of AE events is caused by quartz phase transition (in the silicate aggregate) from triclinic system to the hexagonal system (β at α 573 °C) after heating up to 600 °C (see Fig. 5.15). This resulted, together with the influence of the difference in

the thermal expansion disruption bonds between aggregate and cementing compound, in the creation of a small number of microcracks during the 3PB test. When the heating temperature is increased to 800 °C, the second phase of C-S-H and also of calcium carbonate [$CaCO_3 \rightarrow CaO + CO_2$] decomposition begins. This decomposition leads to a decrease in the number and size of arising microcracks (see Fig. 5.15). In conjunction with the total decomposition of the cementing compound at the temperature of 1000 °C, the lowest value of the number of AE events (the smallest number of arising microcracks) was recorded for the specimens labelled 1000. For the specimens exposed to a thermal stress at a temperature of 1200 °C, a larger number and size of the microcracks formed were recorded again. This is due to a structural change, accompanied by the creation of new crystal phases [Wollastonite β ($CaO.SiO_2$)], which takes place in the specimen's structure at temperatures of above 1000 °C (Bian 2016, Gao 2016).

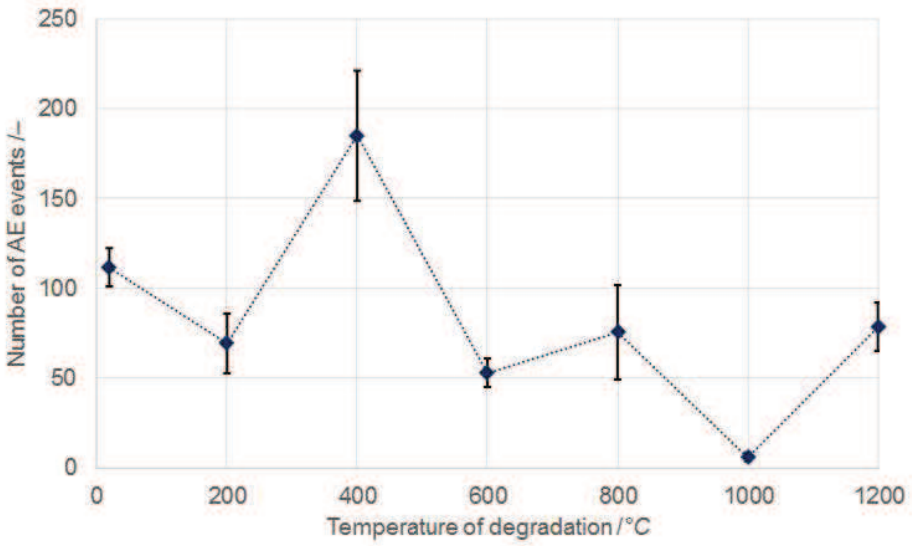

Fig. 5.14. The dependence of the number of AE events on thermal stress level (record to ultimate tensile capacity)

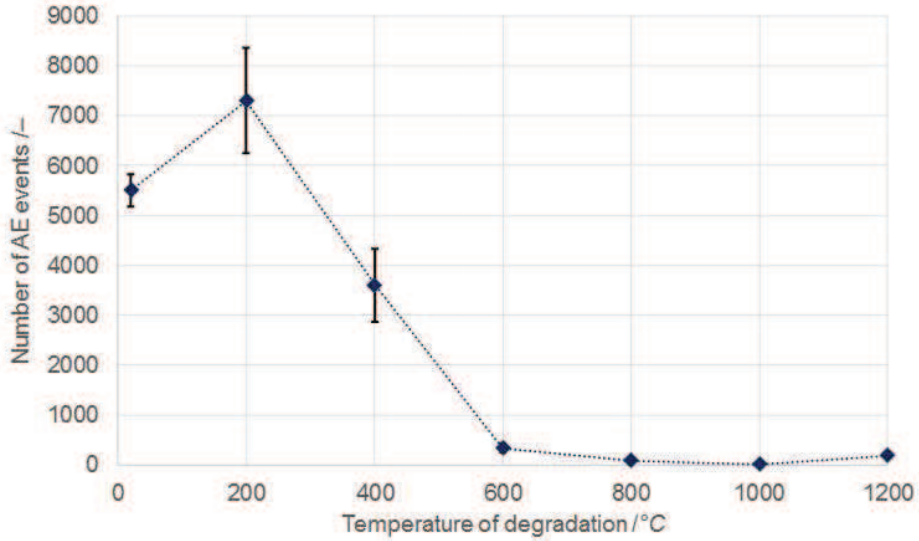

Fig. 5.15. The dependence of the number of AE events on thermal stress level (complete record of the measurement)

The values of AE energy (Fig. 5.16) are in correlation with the toughness of the particular set of concrete specimens. The highest value of AE energy was recorded for specimens exposed to the temperature of 200 °C which may indicate that also the toughness of the specimen is high (in comparison with unheated specimens labelled 20). This implies that structural changes prevent the crack growth because more energy is needed for fracture. Generally speaking, the rising heating temperature above 200 °C causes a decrease in the quantity of AE energy released during the three-point bending test that indicates the raising brittleness of the material. This behaviour of concrete is changed with a temperature of above 1000 °C when the Wollastonite is created and an increase in concrete toughness can be observed.

Figure 5.17 shows the evolution of the dominant frequency of longitudinal temperature-dependent waves. The longitudinal waves that propagate within the specimen can affect the mortar element oscillations. The exposure of a specimen to elevated temperatures causes a decrease of the dominant frequency, which leads to the conclusion that the material's elastic modulus for each composition also decreases. In the course of the degradation, the predominant frequencies are shifting towards the lower frequency range (Štefková 2016).

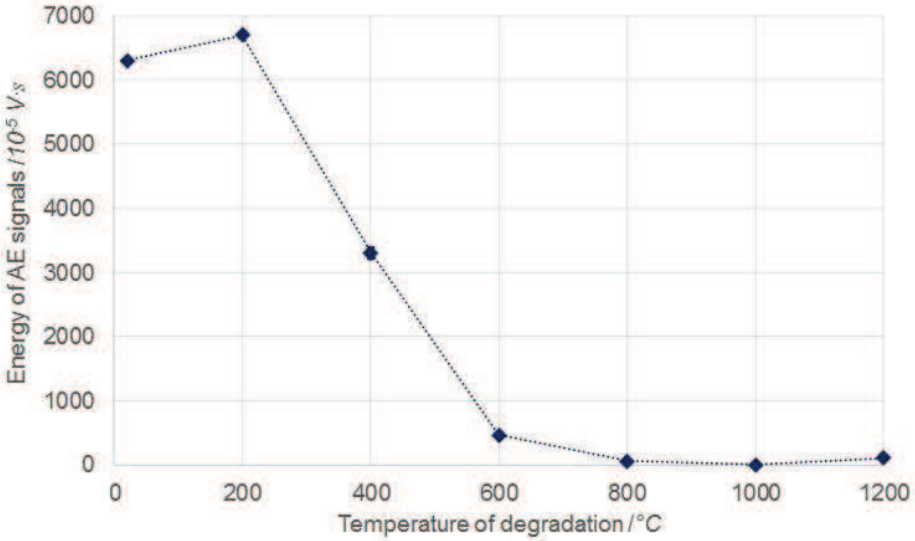

Fig. 5.16. The dependence of energy of AE signals on the degradation thermal stress level (complete record of the measurement)

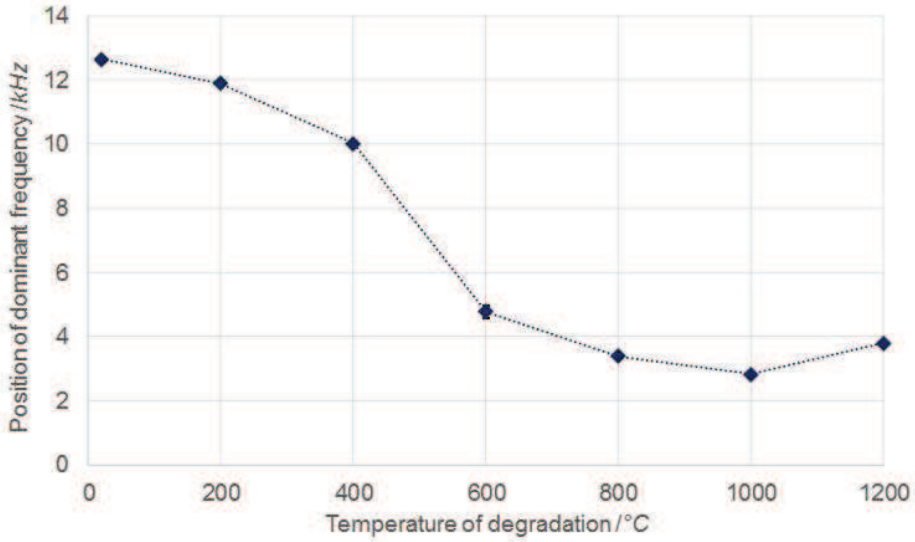

Fig. 5.17. The dominant frequency of longitudinal waves depending on the degradation thermal stress level

5.5 Conclusions

A combination of AE and IE methods is a powerful tool for detecting microcracks in building materials. While the AE method detects active (newly created) microcracks, the IE method detects the passive (already generated) ones. It can be assumed that higher numbers of microcracks cause a greater number of AE events and more numerous dominant frequencies in the frequency spectrum of the IE method.

In selected cases of measuring the setting of cured and uncured concrete specimens, the cyclic loading by freezing, and the thermally degraded specimens, the capacities are declared of both selected non-destructive testing methods, the one of acoustic emission as well as that of impact echo. Particularly the AE method makes it possible to describe the processes going on in the structure of an observed specimen on a continual basis.

Acknowledgement

This outcome has been achieved with the financial support of the project No. LO1408 "AdMaS UP - Advanced Materials, Structures and Technologies", supported by Ministry of Education, Youth and Sports under the „National Sustainability Programme I".

References

Bian H., Hannawi K., Takarli M., Molez L., Prince W., *Effects of thermal damage on physical properties and cracking behavior of ultrahigh-performance fiber-reinforced concrete*, Journal of Materials Science, 2016, vol. 51, issue 22, pp. 10066-10076.

Birgham E., *Fast Fourier Transform and Its Applications*, Prentice Hall, New Jersey, USA 1988.

Brigante M., Sumbatyan M.A., *Acoustic methods for the nondestructive testing of concrete: A review of foreign publications in the experimental field*, Russian Journal of Nondestructive Testing, 2013, vol. 49, issue 2, pp. 100-111.

Gao X., Zhang A., Li S., Sun B., Zhang L., *The resistance to high temperature of magnesia phosphate cement paste containing wollastonite*, Materials and Structures, 2016, vol. 49, issue 8, pp. 3423-3434.

Grosse C., Ohtsu M., *Acoustic Emission Testing*, Springer, Berlin, Germany 2008,.

Ohtsu M., *The history and development of acoustic emission in concrete engineering*, Magazine of Concrete Research, 1996, vol. 48, issue 177, pp. 321–330.

Iturrioz I., Lacidogna G., Carpinteri A., Lacidogna A., *Carpinteri: Acoustic emission detection in concrete specimens: Experimental analysis and lattice model simulations*, International Journal of Damage Mechanics, 2014, vol. 23, issue 3, pp. 327-358. DOI: 10.1177/1056789513494232

Iwanami M., Kamada T., Nagataki S., *Application of acoustic emission technique for crack monitoring in RC beams,* JCA Proc. Cement and Concrete, 1997, vol. 51, pp. 192-197.

Li Z., Xi Y., *Application of acoustic emission technique to detection of concrete cracking and rebar corrosion*, *NDT-CE: Int. Symposium Non-Destructive Testing in Civil Engineering*, Berlin, Germany, 1995,.

Liang M.T., Su P.J., *Detection of Corrosion Damage of Rebar in Concrete Using Impact-Echo Method*, Cement & Concrete Research, 2001, vol. 31, pp. 1427-1436. DOI: 10.1016/S0008-8846(01)00569-5

Pazdera L., Topolář L., Bílek V., Smutný J., Kusák I., Luňák M., *Measuring of Concrete Properties during Hardening*, in Proceedings of the 48th International Scientific Conference on Experimental Stress Analysis, Velke Losiny, Czech Republic, 2010.

Pazdera L., Topolar L., *Application acoustic emission method during concrete frost resistance*, Russian Journal of Nondestructive Testing, 2014, vol.50, issue 2, pp. 127-131. DOI: 10.1134/S1061830914020065

Sagar R.V., *An experimental Study on Acoustic Emission Energy and Fracture Energy of Concrete*. National Seminar & Exhibition on Non-Destructive Evaluation, India, 2009.

Surgeon M., Wevers M., *Modal analysis of acoustic emission signals from CFRP laminates*, NDT & E International, 1999, vol. 32, issue 6, pp. 311-322. DOI: 10.1016/S0963-8695(98)00077-2.

Štefková D., Timčaková K., Topolář L., Cikrle P., *Evaluation of the degree of degradation using the impact-echo method in civil engineering*, *Materiali in tehnologije*, 2016, vol. 50, issue 6, pp. 879-884. DOI: 10.17222/mit.2015.150.

Topolář L., Šimonová H., Misák P., *Effect of Concrete Mixture Composition on Acoustic Emission and Fracture Parameters Obtained from Three-Point Bending Test*, Advanced Materials Research, 2015, vol. 1100, pp. 152-155.

Zhang Y.M,, Chen S.X., Chen B., Sun W., *Dry shrinkage, frost resistance and permeability of rubber included concrete*, Key Engineering Materials, 2006,Vol. 302, pp. 120-124.